ELECTRO-OPTICAL PROPERTY OF EXTREMELY STRETCHED SKINNED MUSCLE FIBERS

YOSHIKI UMAZUME *and* SATORU FUJIME

From the Department of Physiology, The Jikei University School of Medicine, Tokyo 105, Japan. Dr. Fujime's present address is the Department of Physics, Faculty of Science, Nagoya University, Nagoya 464, Japan.

ABSTRACT   Skinned fibers of frog semitendinosus muscle could easily be stretched up to 8 μm or more in sarcomere length. Such extremely stretched fibers gave quite sharp optical diffraction patterns. The intensities of all observable diffraction lines were found to increase on application of electric field (10 ~ 100 V/cm) parallel to the fiber axis, provided that there was no overlap between thin and thick filaments. By use of a polarizing microscope, it was concluded that I-bands were mainly responsible for this intensity increase. By application of square pulses, the time course of the intensity increase and decay was followed. The analysis based on a simple model suggests: (a) Each thin filament has a permanent dipole moment and the moment directs from Z-bands to the free end of the thin filament. (b) The flexural rigidity of thin filaments is estimated to be 2 ~ 3·10^{-17} dyn·cm^2. The present fibers will provide various applications in physicochemical studies of in vivo thin and thick filaments.

INTRODUCTION

Skeletal muscle fibers act as a one-dimensional grating to light, because regularly spaced repetitive striation is due to the periodic change in the refractive index along the fiber axis. Optical diffraction studies of muscle fibers have extensively been made by many authors.

Skinned muscle fibers can be stretched over the sarcomere length of 5 μm (1). Recently Umazume found that skinned fibers of semitendinosus muscle of frogs could be stretched up to 8 μm or more in the sarcomere length (L) and these extremely stretched fibers gave quite sharp diffraction patterns (2). Furthermore, he found that the intensity of the first-order reflection became weaker than that of the second-order reflection at sarcomere lengths longer than 6 μm. This phenomenon could be understood from a simple theoretical consideration by Fujime (3).

In this communication, we wish to present the results that the intensity increase of diffraction lines of extremely stretched fibers was observed on application of electric field and that this phenomenon could be interpreted from a simple physical basis.

MATERIALS AND METHODS

Preparation of Skinned Fibers

Semitendinosus muscle of frogs (*Rana catesbeiana*) was used. A single fiber was dissected by sharp forceps and was placed on a slide glass. The fiber on the slide glass was quickly covered
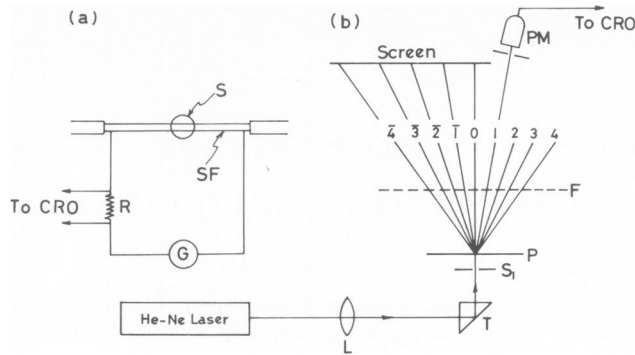
FIGURE 1 Schematic illustration of experimental setup. (a) Application of electric field to a skinned fiber *SF*. *S*, spot of the incident beam (0.3 mm in diameter); *R*, 10 kΩ resistor, *G*, square pulse generator; and CRO, cathode ray oscilloscope. (b) Diffractometer. *L*, lens; *T*, total reflection prism; S_1, slit with a 1 mm in diameter pin hole; *P*, position of a fiber; *F*, position of film loading if necessary; and PM, photomultiplier tube. Arabic numerals show the order of diffraction lines.

with a layer of liquid paraffin oil. To prepare skinned fibers, Natori's method was applied (4). After removal of sarcolemma, the fiber was stretched. A skinned fiber of semitendinosus muscle can easily be stretched up to 8 μm or more in the sarcomere length (2). The frictional force between the slide glass and the fiber kept the stretched sarcomere length unaltered.

Application of Electric Field

Two thin silver wires attached to the surface of the skinned fiber were connected to a stimulator (Nihonkoden, Tokyo; Model MSE-3) *via* a 10-kΩ resistor as a current monitor (Fig. 1a). Square pulses of 20–180 V in height and of 100–500 ms in duration were applied to the wire electrodes separated at 10–15 mm.

Optical Diffractometer

Fig. 1 b is a schematic illustration of our diffractometer. A light beam from a He-Ne laser (NEC, Tokyo; Model 2026; 2 mW nominal) was focused by a lens *L* onto the fiber position *P*. The beam size at the fiber position was about 0.3 mm in diameter. A 1 mm in diameter slit S_1 eliminated undesired light. Diffraction lines were projected on a white screen (sample-to-screen distance; 200 mm), on which we could monitor the diffraction lines. The first-order diffraction line was received by a photomultiplier tube (Hamamatsu TV, Hamamatsu; 1P28) and the output of the tube was fed to an oscilloscope (Nihonkoden, Model VC 7). In photographic recording of diffraction patterns, a photographic film was placed at the position *F* in Fig. 1 b.

Polarizing Microscope

A microscope (Nikon, Tokyo; Apophot) was used. This microscope was equipped with a rectified optical system of Inoué and Hyde's type (5). Photographic films (Kodak Tri-X) were used.

RESULTS

Diffraction Patterns

Fig. 2 shows examples of diffraction patterns. At *L* = 2.9 μm, the intensity of the first-order reflection was higher than that of the second-order reflection (Fig. 2 a). At *L* =
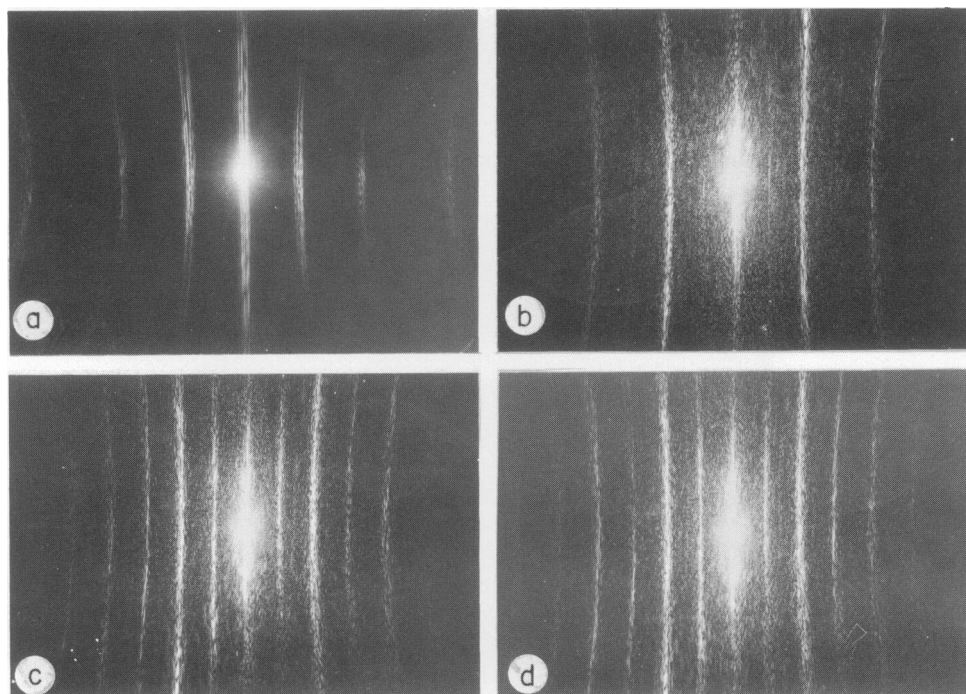
FIGURE 2 Examples of diffraction patterns. (*a*) L = 2.9 μm, (*b*) L = 8.0 μm, (*c*) electric field of 80 V/cm was applied to *b*, and (*d*) applied field was reversed. Note that the specimen-to-film distance was different in *a* and others.
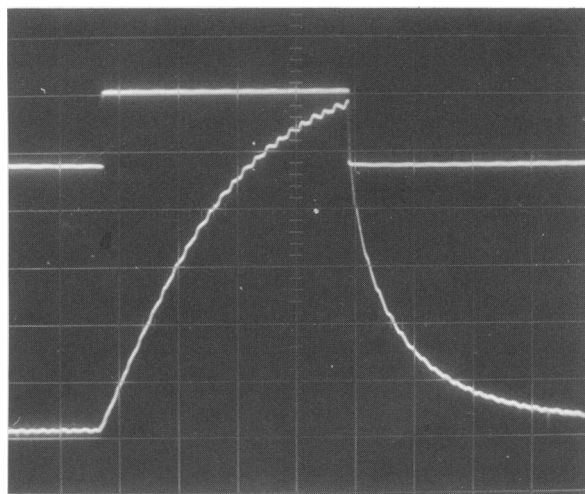

FIGURE 3 An example of intensity increase and decay of the first-order reflection. Upward deflection means the increase in ΔI. Noise on ΔI was due to 100 Hz hum of laser light. L = 8.4 μm, E = 50 V/cm, and horizontal scale: 50 ms/div.

8.0 μm, on the other hand, the intensity of the first order reflection became weaker than that of the second-order reflection (Fig. 2 b). This reversal of intensities can be understood on the basis of Eq. 16 in Appendix I (2,3). Qualitatively speaking, the low/high intensity of the first-/second-order reflection comes from the destructive/constructive contribution of the first and the second terms in Eq. 16. The widths of corresponding
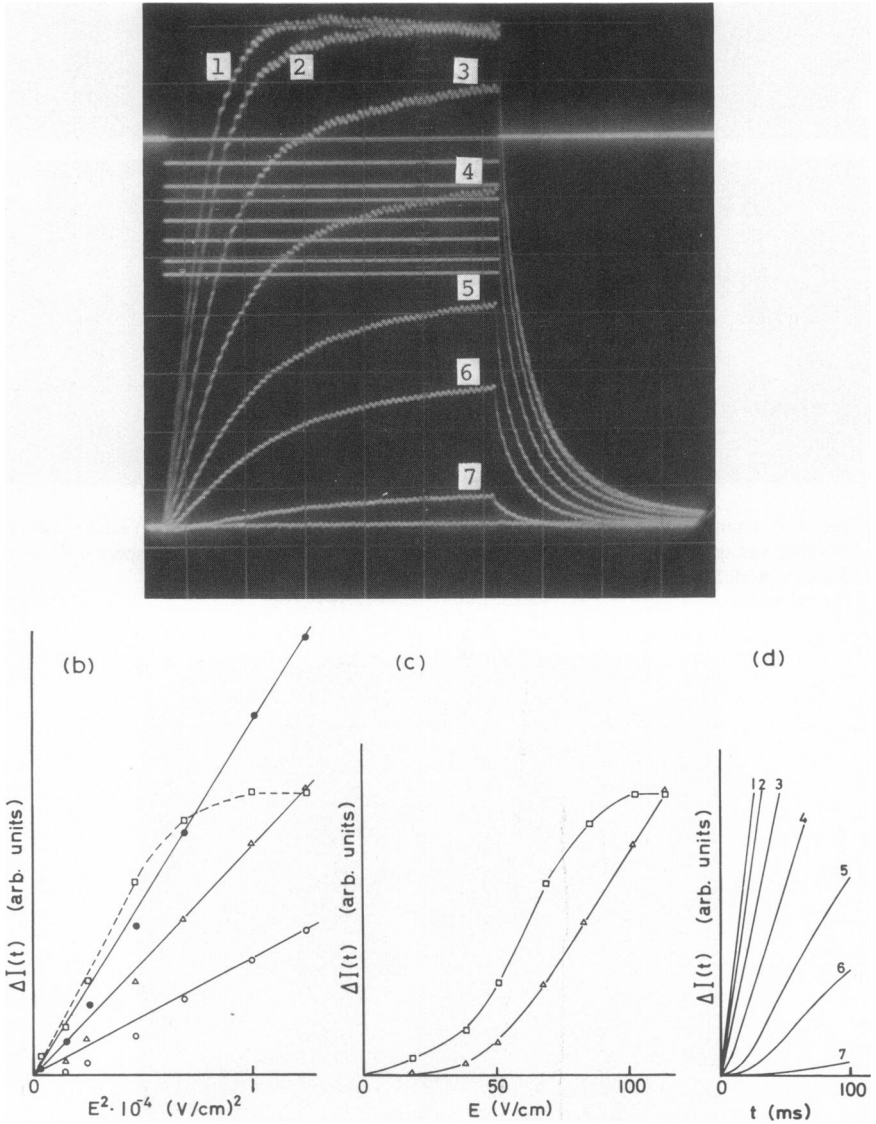

FIGURE 4 ΔI vs. E. $L = 7.5$ μm and horizontal scale: 100 ms/div. (a) Oscilloscope traces of ΔI versus E. (b) $\Delta I(t)$ vs. E^2 at $t = 13$ ms (o), 26 ms ($\triangle$), 39 ms ($\bullet$), and 570 ms ($\square$). (c) $\Delta I(t)$ vs. E at $t = 26$ ms ($\triangle$) and 570 ms ($\square$). (d) Initial portion of a. The t^2 dependence of $\Delta I(t)$ at small t will be seen for low electric field.
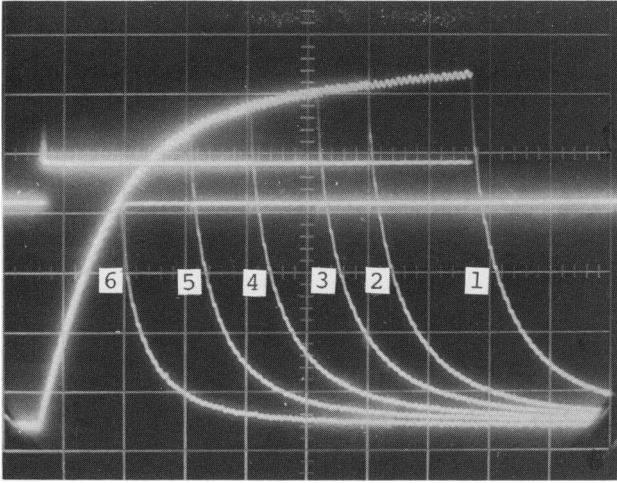
FIGURE 5 ΔI vs. pulse duration time. $L = 7.5\ \mu m$, $E = 60$ V/cm, and horizontal scale: 100 ms/div.

diffraction lines at $L = 2.9\ \mu m$ and $L = 8.0\ \mu m$ were nearly the same. This fact means that the disordering of sarcomere lengths at $L = 8.0\ \mu m$ was somewhat larger than that at $L = 2.9\ \mu m$, because the scattering angle at $L = 8.0\ \mu m$ was much smaller than that at $L = 2.9\ \mu m$. When the fiber was once stretched up to, say, $L = 7\ \mu m$ and then was fixed at $L = 6\ \mu m$, the width of each diffraction line somewhat increased. This prob-
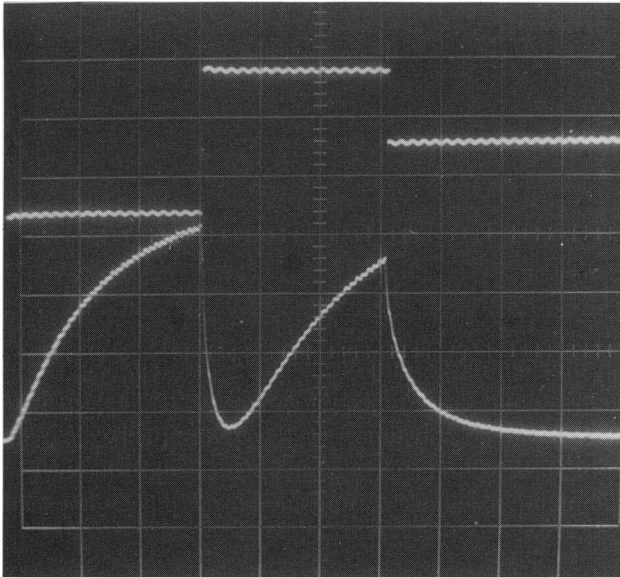

FIGURE 6 $\Delta I(t)$ on application of a reversed pulse. $L = 8.4\ \mu m$, $E = 60$ V/cm, and horizontal scale: 100 ms/div.

ably suggests that the extreme stretching made the partial damage of a parallel elastic component supporting the relative positions of myofilaments in myofibrils. On application of electric field E parallel to the fiber axis, the intensities of all observable reflections increased independently of the polarity of the applied field (Figs. 2 c and d). In this intensity increase, no appreciable change in widths of diffraction lines was observed. In photographs in Figs. 2 c and d, great increases of intensities of the first- and third- to sixth-order reflections are observed relative to the intensity of the second-order reflection. Since the intensity of the second-order reflection was very high, its increase on application of electric field was not prominent. However, it did increase. The intensity increase of diffraction lines on application of electric field could be observed only when muscle fibers were stretched so that there was no overlap between thin and thick filaments. The extremely stretched fiber could not contract on Ca^{2+}-injection. However, when the contact between the fiber and the slide glass was removed, the length of the fiber shortened and diffraction lines broadened. Such a fiber could contract on Ca^{2+}-injection. The intensity increase could be observed repeatedly and its extent was nearly the same even after the fiber was left standing at room temperature for 24 h.

The Time Course of the Intensity Increase on Application of Electric Square Pulse

Fig. 3 shows an example of the intensity increase $\Delta I(t)$ of the first-order reflection on application of a square pulse. The gradual increase and rapid decay of the intensity are clearly seen.
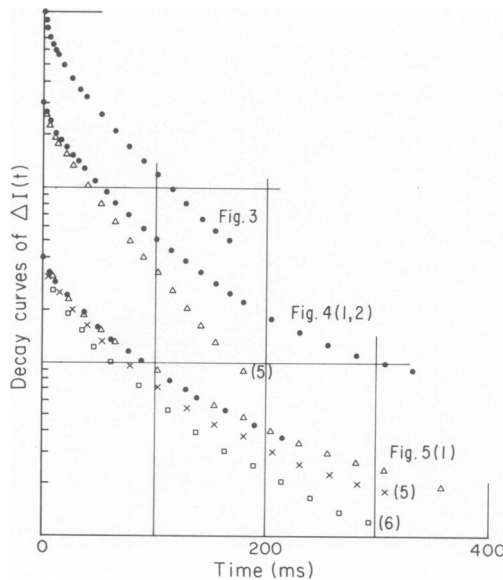
FIGURE 7   Semi-logarithmic plots of decay curves in Figs. 3, 4, and 5.

Fig. 4 *a* shows the relationship between ΔI and E. Fig. 4 *b* shows the relationship between $\Delta I(t)$ at various times and E^2. The initial slope is proportional to E^2. Fig. 4 *c* shows the relationship between ΔI and E.

Fig. 5 shows the relationship between $\Delta I(t)$ and pulse duration time. The rising curves completely overlapped. Fig. 6 shows the intensity change on application of a reversed pulse.

Fig. 7 shows semi-logarithmic plots of decay curves of $\Delta I(t)$ in Figs. 3, 4, and 5. All of these decay curves consist of at least two exponentials:

$$\Delta I(t) = Ae^{-t/\tau_f} + Be^{-t/\tau_s}, \tag{1}$$

where suffices *f* and *s* refer to fast and slow components, respectively. Application of high field for a long time results in the increase of the slow component (B). The results of the computer analysis using Eq. 1 are given in Table I.

Fig. 8 shows the behavior of the intensity increase on application of reversal pulses. Just after the inversion of polarity of the pulse, the intensity increase occurred in a

TABLE I
TWO-EXPONENTIAL LEAST SQUARE ANALYSIS OF DECAY CURVES

Sample	τ_f	τ_s	A	B	Remarks*	
					T	E
	ms	*ms*	%	%	*ms*	*V/cm*
Fig. 3	4.5 ± 1	60 ± 2	33	66	200	50
Fig. 4 (1, 2)	10.0 ± 2	82 ± 5	34	65	↑	110
(3)	10.0 ± 2	74 ± 3	34	65		80
(4)	3.8 ± 1	62 ± 3	23	76	570	70
(5)	4.9 ± 1	56 ± 2	23	76		50
(6)	3.6 ± 1	51 ± 2	23	76	↓	40
Fig. 5 (1)	9.7 ± 1	100 ± 5	33	66	700	↑
(2)	20.0 ± 2	126 ± 6	47	52	530	
(3)	22.0 ± 2	136 ± 6	51	48	460	60
(4)	18.0 ± 2	136 ± 8	51	48	350	
(5)	11.0 ± 2	108 ± 8	45	54	250	
(6)	6.2 ± 1	80 ± 5	44	55	140	↓
4P16‡ (1)	13.0 ± 3	105 ± 7	37	62	700	↑
(2)	16.0 ± 3	120 ± 8	43	56	600	
(3)	21.0 ± 5	126 ± 20	54	45	510	
(4)	21.0 ± 2	138 ± 10	63	36	420	70
(5)	8.5 ± 1	77 ± 4	32	67	320	
(6)	11.0 ± 2	77 ± 5	41	58	230	
(7)	12.0 ± 1	77 ± 5	46	53	140	↓
4P01‡	8.2 ± 1	77 ± 6	63	36	200	60

*E, applied field; T, duration time of applied field.
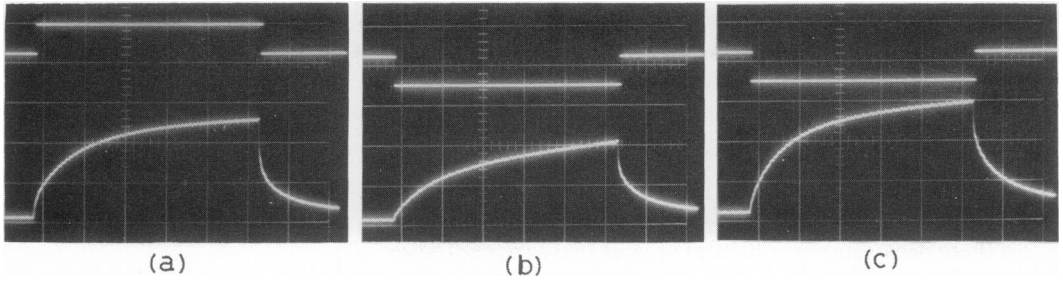‡ Original curves are not shown in the text.

FIGURE 8 Photographs showing aftereffect due to multiple application of electric field of the same polarity. (a) at the 20th pulse of the same polarity, (b) at the first reverse pulse, and (c) at the 15th reverse pulse. Pulse interval: about 10 s, $L = 7.5 \mu m$, $E = 80$ V/cm, and horizontal scale: 100 ms/div.

quite different manner. The rising curve almost consists mainly of the slow component, whereas the decay curve is similar to that of the previous curve. There was an aftereffect due to multiple application of electric pulses of the same polarity. After application of several pulses, the total behavior of ΔI returned to that before the polarity change.

An analysis suggested that the resistance of the fiber (in Fig. 4) was about 13 MΩ or the specific resistance of about 100 Ωcm. This value corresponds to the specific resistance of a 0.1 M KCl solution. In our usual cases, the fiber resistance was of the order of 10 MΩ and applied voltage of 100 V, so that a pulse of 300 ms duration produced joule heat of 0.7 mcal. The volume of the fiber where current flowed was of the order of $(\pi/4)(50 \mu m)^2(1.5$ cm$) = 3 \cdot 10^{-5}$ ml. This volume of water is expected to be heated up to 20°C or more by one pulse. Owing to the effect of a heat sink of paraffin
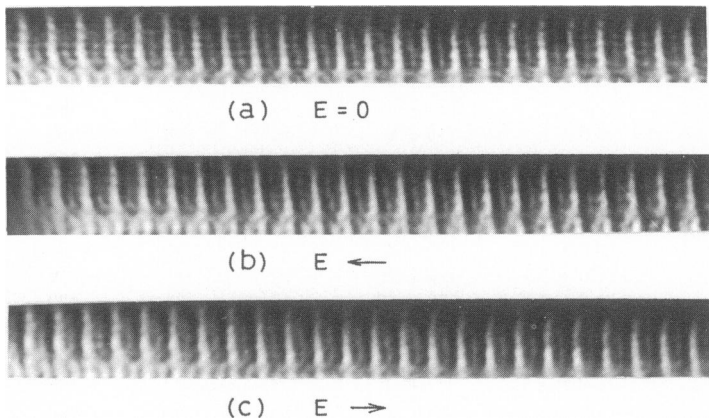

FIGURE 9 Polarizing micrographs. (a) control ($E = 0$), (b) $E = 70$ V/cm, and (c) $E = 70$ V/cm reversed to b. $L = 6.0 \mu m$.
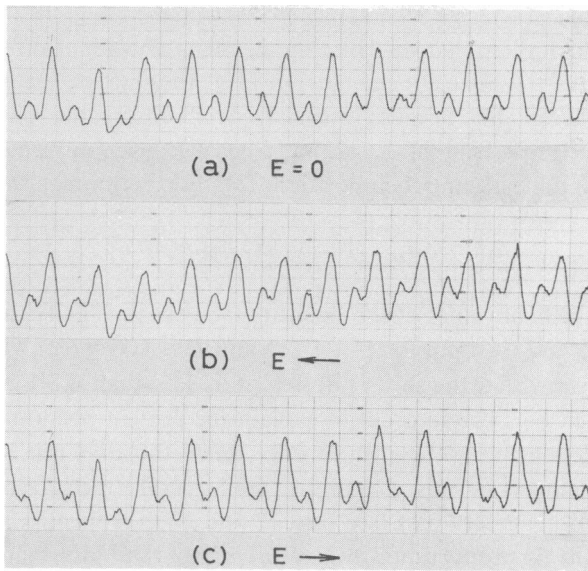
FIGURE 10   Densitometer traces of micrographs in Fig. 9.

oil covering the fiber, however, it is supposed that the fiber was in fact not very much heated.

Studies by Use of Polarizing Microscope

In order to see which bands were mainly responsible for the intensity increase, I-bands or A-bands, the fiber was studied by use of the polarizing microscope.   Fig. 9 shows some examples of micrographs taken by use of Apophot.   The optical system was set so as the non-birefringent portion gave black contrast.   Thus, in Fig. 9, the bright bands show A-bands, dark bands show I-bands, and black bands show the non-birefringent portions (i.e., the intracellular solution).   Fig. 10 shows the densitometer traces of micrographs.   On application of electric field, the black bands on one side of I-bands became more black than those on the other side of I-bands.   Due to this fact, microscopic observations gave impression that I-bands shift phoretically.   From Fig. 10, however, the shift of I-bands, if present, is estimated to be less than 0.3 μm. From these Figs, the main change was seen to occur not in A-bands but in I-bands. Moreover, this change depended on the polarity of applied field.   This fact indicates that Ca^{2+}–release from the internal membrane system stimulated by electric pulse is not an origin of the present phenomenon.   At the sarcomere length of about 3.8 μm, partial occurrence of the above phenomenon was observed.

DISCUSSION

It can be supposed from Figs. 9 and 10 that, on application of electric field, the degree of birefringence of, and the refractive index of, I-bands right (left) to Z-bands increase,

or *I*-bands shift by $+(-)\xi$, as schematically illustrated in Fig. 12 in Appendix. As shown in Appendix I, these changes cause the intensity change of diffraction lines. As to the main origin of the intensity change, however, the shift of *I*-bands by more than 1 μm can not be acceptable, because intensities of all observable reflections increased on application of electric field (cf. Eq. 22) and because, even in isometric contraction, *I*-bands do not fluctuate around their positions (3). Furthermore, although Eq. 22,

$$\Delta I_c \propto 1 - \cos(2\pi[\xi/L])$$ (2)

seems to explain the final values of the intensity increase in Fig. 4 *c*, it is not likely because Eq. 2 results in $\xi = 4$ μm for $L = 8$ μm and $E = 100$ V/cm. The densitometer traces in Fig. 10 show that the shift ξ, if present, is less than 0.3 μm. Therefore, we adopt the model in Fig. 12 *b* in order to explain the present phenomenon. As to this problem, the following must be mentioned: Since the unit cell has no center-of-symmetry in our models in Figs. 12 *b* and *c*, the structure factor $F(n)$ becomes complex, i.e., it has an imaginary part (see Eqs. 17 and 20 in Appendix I). However, the diffraction intensity is proportional to $|F(n)|^2$, so that information on phase of the scattered wave is absent in intensity data themselves. (This is the sole reason why the intensity increase of diffraction lines on application of electric field did not depend on polarity of the applied field.) If we compute the Fourier series

$$n(x) = \sum_{n=0}^{n'} F(n)e^{-2\pi i(x/L)n},$$ (3)

with $F(n) = F_b(n)$ or $F_c(n)$ in Appendix I and n' determined by the numerical aperture of our microscope, and if the computed $n(x)$ values were compared with the densitometer traces in Fig. 10, we could decide which model is better, Fig. 12 *b* or *c*. However, we did not make such simulation because similar experiments on crab muscle favored the model in Fig. 12 *b* (Y. Maéda, personal communication). (The lengths of both *A*- and *I*-bands of crab muscle are much longer than those of frog muscle, so that n' in the above equation is much larger than ours. This means that there are lesser optical artefacts in micrographs of crab muscle than those of present muscle.)

Since there is no overlap between thin and thick filaments, the packing of thin filaments becomes loose at the free end due to the repulsive force between them (Fig. 11 *a*). As to a possible origin of the changes in the degree of birefringence of, and the refractive index of, *I*-bands, we propose that the ordering and disordering of the arrangement of thin filaments. If each thin filament has an electric dipole moment μ parallel to the fiber axis, the torque to orient thin filaments is given by $\mu E \cdot \cos \theta$ where θ is the angle between vectors μ and **E**. Thus the ordering and disordering of thin filaments on application of electric field will be expected (Fig. 11 *b* and *c*). In vitro *F*-actin having the length up to about 1 μm has known to have a large permanent dipole moment parallel to the long axis (6). If the torque to orient the filament is due to the induced dipole moment, it is proportional to E^2, that is, no effect of the polarity change of
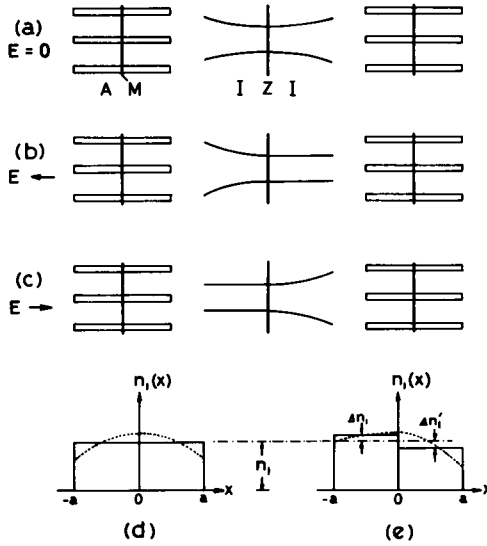
FIGURE 11 Schematic representation of the proposed structure of an extremely stretched fiber. (a) $E = 0$, (b) E = (+) and (c) $E = (-)$. A, thick filament; M, M-line; I, thin filament; and Z, Z-band. (d) . . . . , Assumed value of the refractive index of I-band, $n_I(x)$; and ——, rectangular approximation of $n_I(x)$, $E = 0$. (e) Effect of applied field on $n_I(x)$. See Fig. 12.

applied field will be observed. However, Figs. 6 and 9 show the effect of the polarity. This means that the induced dipole moment, if present, has no appreciable effect on the present phenomenon.

On Rising Curve of $\Delta I(t)$

If we assume that the value of Δn_I ($\Delta n_I'$) is proportional to the degree of ordering (disordering) of thin filaments in I-bands, Δn_I ($\Delta n_I'$) will be proportional to the field strength E. Thus Eq. 19 A gives $\Delta I(t = \infty) \propto E^2$ (□ in Fig. 4 b). At a higher field strength, $\Delta I(t = \infty)$ becomes constant or slightly decreases (Fig. 4 a). This is probably due to the failure of $\Delta n_I = \Delta n_I'$, especially due to the result of $\Delta n_I' > \Delta n_I$ at $t = \infty$ (see Eq. 19). Now, we have for small t and small θ:

$$\Xi(d\theta/dt) = -\mu E \cos\theta \tag{4}$$

and thus

$$\theta(t) = -(\mu E \cos\theta_0/\Xi)t + \theta_0 \tag{5}$$

where Ξ is the friction constant and θ_0 is the initial value of θ. In our model, the initial value of $\Delta n_I(t)$ is expected to be proportional to $\theta_0 - \theta$:

$$\Delta n_I = \Delta n_I' \propto (\mu E \cos\theta_0/\Xi)t \qquad \text{(for small } t\text{).} \tag{6}$$

Then we have from Eqs. 19 A and 6:

$$\Delta I(t) \propto (\Delta n_I)^2 \propto (\mu E \cos\theta_0/\Xi)^2 t^2, \tag{7}$$

and

$$[d\Delta I(t)/dt] \propto (\mu E \cos\theta_0/\Xi)^2 t. \tag{8}$$

This means that the initial slope of the rising curve of $\Delta I(t)$ is proportional to E^2 (Fig. 4 b). However, Fig. 4 suggests that $\Delta I(t) \propto E^2 t$ (for small t). This is due to the rapid disappearance of the t^2 dependence of $\Delta I(t)$. (In Fig. 4 d, slight traces of the t^2 dependence are seen.) In crab muscle where the present phenomenon is very prominent, the complete t^2 dependence is observed for $t \leq 15$ ms although slow sweep data are quite similar to those in Fig. 4 (Y. Maéda, personal communication).

On Decay Curve of $\Delta I(t)$

If the change of $\Delta n_I(t)$ in Appendix I after removal of electric field is assumed to follow

$$\Delta n_I(t) = \Delta n_I e^{-t/\tau}, \tag{9}$$

then Eq. 19 A gives

$$\Delta I(n,t) \propto (1/n^2)\sin^4[\pi(a/L)n](\Delta n_I)^2 e^{-2t/\tau}. \tag{10}$$

The relaxation times shown in Table I are roughly divided into three classes; the first is $\tau_f \simeq 5$ ms and $\tau_s \simeq 60$ ms, the second is $\tau_f \simeq 10$ ms and $\tau_s \simeq 80$ ms, and the third is $\tau_f \simeq 20$ ms and $\tau_s \simeq 130$ ms. This fact suggests that many processes occurred on application of electric field. The first class was observed for fresh fibers at low E and/or short T. We assume that data of the first class reflect the primary process of the present phenomenon. If we equate Eq. 10 with the fast component of Eq. 1, we have the relation $\tau = 2\tau_f$.

Although not clear, it is inferred that $\Delta n'_I(t)$ has the slow relaxation time and considered to be the origin of the slow component. This explanation is expected, because Fig. 7 indicates that fractions of the slow component are small at small E values and at short duration of pulses, and because Fig. 6 indicates that the rising curve on application of the reversed pulse very much delayed inspite of the acceleration effect of the pulse on returning of the Δn_I and $\Delta n'_I$.

As to the slow relaxation time τ_s in Eq. 1, the following possibilities can not completely be excluded at present: (1) The positions of A-bands and/or I-bands are phoretically shifted by a small distance ξ against a parallel elasticity, i.e., a part acceptance of the model in Fig. 12 c, and (2) Some higher-order rearrangements occur as a result of the inhomogeneity of applied electric field.

On Flexibility of Thin Filaments

Now, the lowest order relaxation time τ_1 of lateral fluctuations of a rod with length 1 μm, of which one end is clamped and the other end is free, is given by

$$\tau_1 = 3.1 \cdot 10^{-19}/\epsilon \qquad \text{(seconds)} \qquad (11)$$

where ϵ is the flexural rigidity (see Appendix II). The fluctuation-dissipation theorem (7) says that $\tau_1 = \tau$. Then the assumption of $\tau_1 = \tau(=2\tau_f)$ gives $\epsilon = 2 \sim 3 \cdot 10^{-17}$ dyn $\cdot$ cm^2, which is very close to $\epsilon = 2 \cdot 10^{-17}$ dyn $\cdot$ cm^2 estimated from in vitro experiments of F-actin by quasi-elastic scattering of laser light. (8).

From Eq. 36 (in Appendix III) and the estimated values of $\epsilon = 2 \sim 3 \cdot 10^{-17}$ dyn $\cdot$ cm^2, the mean amplitude of lateral fluctuations of thin filaments is estimated to be $\langle \delta^2 \rangle = (140 \sim 170 \text{ nm})^2$. Owing to such a large amplitude, fluctuations of thin filaments could be detected by forward diffraction (scattering) of light. Although the theoretical considerations in Appendices II and III are concerned with a single filament (or a dilute solution), the above estimated values are believed to have at least qualitative meanings. Thin filaments in the overlap region can not fluctuate in such a large amplitude as above, because of restriction due to surrounding thick filaments. However, the present result suggests the flexibility of thin filaments. Thin filaments are not rigid but semiflexible as has previously been stressed on the basis of in vitro experiments (8).

Concluding Remarks

The increase of flexibility of a reconstituted thin filament, i.e., an F-actin/tropomyosin/troponin complex, is observed on addition of Ca^{2+} more than 1 μM (9). This flexibility increase is greatly amplified by addition of (heavy mero)myosin (10, 11). From the present result, it is inferred that the flexibility change of in vivo thin filaments occurs as in the case of in vitro thin filaments and that this flexibility change surely plays important roles in muscle contraction (11).

The same effect of applied field on thick filaments is also expected. However, thick filaments of frog muscle are too stiff and too short for the observation of such an effect. Eq. 35 in Appendix III shows that $\langle \delta^2 \rangle \propto l^3/\epsilon$. If the similar study as the present one were made on, for example, crab muscle, the flexural rigidity of thick filaments could also be determined.

In vitro reconstitution of both thin and thick filaments has partly been succeeded, and extensive studies have been made by use of in vitro filaments. However, in vitro reconstitution of neither I-bands nor A-bands has been succeeded. In such a situation, the present fibers will provide various application in physicochemical studies of in vivo I- and A-bands as well as thin and thick filaments.

APPENDIX I

Denote by $F(h)$ the structure factor of a unit cell. Then we have the total scattering amplitude of the fiber:

$$S(h) = F(h) \sum_{j=0}^{N} e^{2\pi i h L j} = F(h) \Phi(h) \mathcal{L}(h), \tag{12}$$

where N is the number of unit cells in an illuminated region of the fiber, L is the sarcomere length, $|\Phi| = |\exp(\pi i h N L)/\exp(\pi i h L)| = 1$ and, for large N, the Laue function $\mathcal{L}(h) = \sin(\pi h N L)/\sin(\pi h L)$ becomes

$$\mathcal{L}(h) = N \qquad \text{for } h = n/L \qquad (n: \text{integers}),$$
$$= 0 \qquad \text{otherwise.}$$

Thus the scattered intensity $I(n)$ of the nth order reflection is given by

$$I(n) \propto |S(n)|^2 = N^2 |F(n)|^2. \tag{13}$$

The structure factor $F(h)$ is given by

$$F(h) = \int_{-L/2}^{L/2} n(x) e^{2\pi i h x} dx. \tag{14}$$

For the unit cell structure in Fig. 12 a, we have (3):

$$F_a(n) = \left(\exp\left[2\pi i \frac{n}{L}\left(-\frac{a}{2} \right) \right] + \exp\left[2\pi i \frac{n}{L}\left(\frac{a}{2} \right) \right] \right)$$

$$\cdot \int_{-a/2}^{a/2} n_I \exp\left(2\pi i \frac{n}{L} x \right) dx$$

$$+ \left(\exp\left[2\pi i \frac{n}{L}\left(-\frac{2L - b}{4} \right) \right] + \exp\left[2\pi i \frac{n}{L}\left(\frac{2L - b}{4} \right) \right] \right)$$

$$\cdot \int_{-b/4}^{b/4} n_A \exp\left[2\pi i \frac{n}{L} x \right] dx$$

$$= \frac{L}{n\pi}\left[n_I \sin\left(\pi \frac{2a}{L} n \right) + (-1)^n n_A \sin\left(\pi \frac{b}{L} n \right) \right], \tag{15}$$
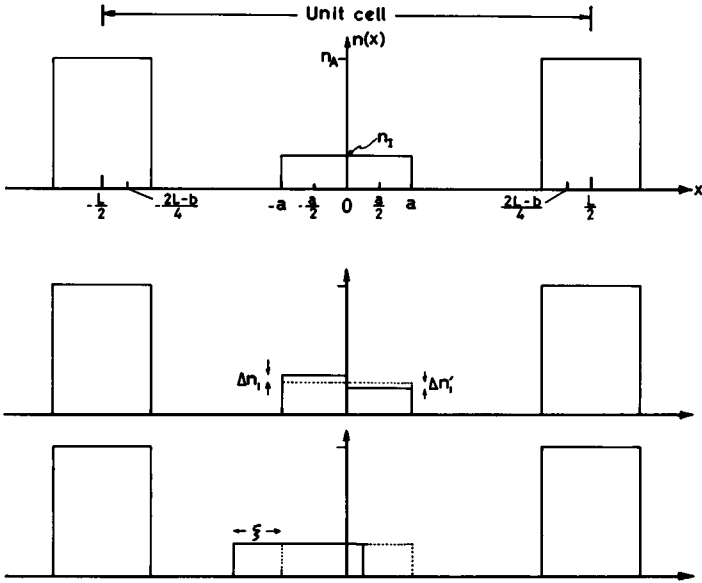
FIGURE 12 Schematic representation of the assumed structure of the unit cell. (a) $E = 0$, and (b, c) $E \neq 0$. n_A and n_I, refractive indices of A-band and I-band, respectively; Δn_I in b, change of n_I on application of electric field; ξ in c, shift of I-band on application of electric field; a and b, lengths of thin and thick filaments, respectively; and L, sarcomere length.

and

$$I_a(n) = C\frac{1}{n^2}\left[n_I\sin\left(\pi\frac{2a}{L}n\right) + (-1)^n n_A\sin\left(\pi\frac{b}{L}n\right)\right]^2, \tag{16}$$

where C is the proportional constant. For the unit cell structure in Fig. 12 b, we have

$$F_b(n) = F_a(n) + (L/n\pi)(\Delta n_I - \Delta n_I')\cos[\pi(a/L)n]\sin[\pi(a/L)n]$$
$$\pm i(L/n\pi)(\Delta n_I + \Delta n_I')\sin^2[\pi(a/L)n], \tag{17}^1$$

$$I_b(n) = I_a(n) + \Delta I_b(n), \tag{18}$$

and

$$\Delta I_b(n) = C(1/n^2)\{(n\pi/L)F_a(n)\cdot(\Delta n_I - \Delta n_I')\sin[\pi(2a/L)n]$$
$$+ (\Delta n_I^2 + \Delta n_I'^2)\sin^2[\pi(a/L)n]$$
$$+ 2\Delta n_I\Delta n_I'(\sin^2[\pi(a/L)n] - \cos^2[\pi(a/L)n])\sin^2[\pi(a/L)n]\}. \tag{19}$$

If $\Delta n_I = \Delta n_I'$ is assumed, Eq. 19 becomes simple:

$$\Delta I_b(n) = C(4/n^2)(\Delta n_I)^2\sin^4[\pi(a/L)n]. \tag{19 A}$$

---

[1] Double signs $\pm$ in Eqs. 17 and 20 are due to the effect of polarity of applied field.

Finally, for the unit cell structure in Fig. 12 c, we have

$$F_c(n) = (L/n\pi)(n_I \sin[\pi(2a/L)n] \exp[\pm 2\pi i(\xi/L)n]$$
$$+ (-1)^n n_A \sin[\pi(b/L)n]), \qquad (20)^1$$

$$I_c(n) = I_a(n) + \Delta I_c(n) \qquad (21)$$

and

$$\Delta I_c(n) = C \cdot (-1)^n (1/n^2) 2 n_I n_A \sin[\pi(2a/L)n] \sin[\pi(b/L)n]$$
$$\times (\cos[2\pi(\xi/L)n] - 1). \quad (22)$$

It is noted that $\Delta I_b(n)$ in Eq. 19 A is non-negative, i.e. $\Delta I_b(n) \geq 0$, whereas $\Delta I_c(n)$ in Eq. 22 is positive or negative depending on the values of n, a, b, L, and ξ.

APPENDIX II

The spontaneous bending motion of a rod (Fig. 13) in a viscous medium is expressed by the following Langevin equation (12):

$$\rho(\partial^2 \mathbf{r}/\partial t^2) + \zeta(\partial \mathbf{r}/\partial t) + \epsilon(\partial^4 \mathbf{r}/\partial x^4) = \mathbf{A}(x,t), \qquad (23)$$

where ρ is the linear density of, ζ is the friction constant per unit length of, and ϵ is the flexural rigidity of, the rod, and $\mathbf{A}(x,t)$ is the random fluctuating force. By mode expansion:

$$\begin{Bmatrix} \mathbf{r}(x,t) \\ \mathbf{A}(x,t) \end{Bmatrix} = \sum_n \begin{Bmatrix} \mathbf{q}(n,t) \\ \mathbf{B}(n,t) \end{Bmatrix} Q(n,x). \qquad (24)$$

Eq. 23 becomes

$$\rho \ddot{\mathbf{q}}(n,t) + \zeta \dot{\mathbf{q}}(n,t) + \lambda_n \mathbf{q}(n,t) = \mathbf{B}(n,t) \qquad (25)$$

and

$$\epsilon[d^4 Q(n,x)/dx^4] = \lambda_n Q(n,x), \qquad (26)$$

where λ_n is the separation constant. From Eq. 25, we have the relaxation time τ_n as (12)

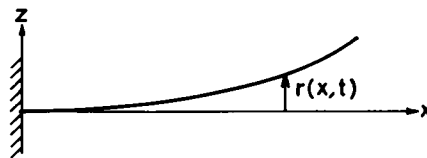$$\tau_n = \zeta/\lambda_n. \qquad (27)$$

FIGURE 13 Definition of coordinates.

Eq. 26 and boundary conditions

$$Q(n,0) = \frac{dQ}{dx}\bigg|_{x=0} = \frac{d^2Q}{dx^2}\bigg|_{x=l} = \frac{d^3Q}{dx^3}\bigg|_{x=l} = 0 \qquad (28)$$

give the secular equation:

$$1 + \cos(\beta l)\cosh(\beta l) = 0, \qquad (29)$$

where $\beta = \sqrt[4]{\lambda_n/\epsilon}$ and l is the length of the rod. The smallest root of Eq. 29 is $\beta_1 l = 0.6\,\pi$, which gives $\lambda_1 = \epsilon\beta_1^4$ or

$$\tau_1 = \zeta/\epsilon\beta_1^4 = (\zeta l \cdot l^3)/\epsilon(0.6\pi)^4 = (\zeta l/kT)kTl^3/\epsilon(0.6\pi)^4, \qquad (30)$$

where k is the Boltzmann constant. Since ζ is defined as the friction constant per unit length, $\zeta l/kT$ is assumed to be the inverse of the translational diffusion constant D of the rod. Putting $l = a = 1\ \mu$m (the length of the thin filament) and $D = 1 \cdot 10^{-8}\,$cm^2/s, we have

$$\tau_1 = (3.1 \cdot 10^{-19})/\epsilon \qquad \text{(seconds)} \qquad (31)$$

For details of the above algebra, see ref. 12.

APPENDIX III

The elastic potential energy $\langle V \rangle$ of the bending motion of a rod is given by

$$\langle V \rangle = \left\langle \frac{1}{2} \int_0^l \epsilon \left(\frac{\partial^2 \mathbf{r}}{\partial x^2}\right)^2 dx \right\rangle$$

$$= \frac{1}{2} \sum_n \sum_m \langle \mathbf{q}(n,t) \cdot \mathbf{q}(m,t) \rangle \int_0^l \epsilon \frac{d^2 Q(n,x)}{dx^2} \cdot \frac{d^2 Q(m,x)}{dx^2}\, dx.$$

Partial integrations using Eqs. 26 and 28 lead to

$$\langle V \rangle = \frac{1}{2} \sum_n \sum_m \lambda_m \langle \mathbf{q}(n,t) \cdot \mathbf{q}(m,t) \rangle \int_0^l Q(n,x) Q(m,x)\, dx.$$

Since $\{ Q(n,x) \}$ is an orthonormal set, it holds that

$$\int_0^l Q(n,x) Q(m,x)\, dx = \delta_{nm}, \qquad (32)$$

where δ_{nm} is the Kronecker delta. Then we finally have

$$\langle V \rangle = \frac{1}{2} \sum_n \lambda_n \langle \mathbf{q}(n,t) \cdot \mathbf{q}(n,t) \rangle. \qquad (33)$$

By equipartition of energy, we have from Eq. 33 that

$$\langle \mathbf{q}(n,t) \cdot \mathbf{q}(n,t) \rangle = 2kT/\lambda_n \tag{34}$$

for two-dimensional fluctuations (along y and z axes in Fig. 13). The mean amplitude $\langle \delta^2 \rangle$ of the lateral fluctuations of the above rod is given by

$$
\begin{aligned}
\langle \delta^2 \rangle &= \frac{1}{l} \int_0^l \langle \mathbf{r}(x,t)^2 \rangle \mathrm{d}x \\
&= \frac{1}{l} \sum_n \sum_m \langle \mathbf{q}(n,t) \cdot \mathbf{q}(m,t) \rangle \int_0^l Q(n,x) Q(m,x) \mathrm{d}x \\
&= \frac{1}{l} \sum_n \frac{2kT}{\lambda_n} \simeq \frac{1}{l} \cdot \frac{2kT}{\lambda_1} = \frac{2kT \cdot l^3}{\epsilon (0.6\pi)^4} .
\end{aligned}
\tag{35}
$$

Assuming again $l = 1\ \mu\mathrm{m}$, we have

$$\langle \delta^2 \rangle \simeq (6 \cdot 10^{-27})/\epsilon \quad \text{(square centimeters)} \tag{36}$$

For details of the above algebra, see also ref. 12.

REFERENCES

1. NATORI, R., Y. UMAZUME, and T. YOSHIOKA. 1974. *Jikeikai Med. J.* **21.** In the press.
2. UMAZUME, Y. 1974. *J. Physiol. Soc. Jap.* **36.** In the press.
3. FUJIME, S. 1974. *Biochim. Biophys. Acta.* In the press.
4. NATORI, R. 1954. *Jikeikai Med. J.* **1:**18.
5. INOUÉ, S., and W. L. HYDE. 1957. *J. Biophys. Cytol.* **3:**831.
6. KOBAYASHI, S., H. ASAI, and F. OOSAWA. 1964. *Biochim. Biophys. Acta.* **88:**528.
7. KUBO, R. 1966. *Rep. Prog. Phys.* **29:**255.
8. FUJIME, S., and S. ISHIWATA. 1971. *J. Mol. Biol.* **62:**251.
9. ISHIWATA, S., and S. FUJIME. 1972. *J. Mol. Biol.* **68:**511.
10. ISHIWATA, S., and S. FUJIME. 1971. *J. Phys. Soc. Japan.* **31:**1601.
11. OOSAWA, F., S. FUJIME, S. ISHIWATA, and K. MIHASHI. 1972. *Cold Spring Harbor Symp. Quant. Biol.* **37:** 277.
12. FUJIME, S., and M. MARUYAMA. 1973. *Macromolecules.* **6:**237.